MAVEN observations of energy-time dispersed electron signatures in Martian crustal magnetic fields

Y. Harada, D. L. Mitchell, J. S. Halekas, J. P. Mcfadden, C. Mazelle, J. E. P. Connerney, J. Espley, D. A. Brain, D. E. Larson, R. J. Lillis, et al.

HAL Id: insu-03670547

https://insu.hal.science/insu-03670547

Submitted on 17 May 2022

Key Points:
- MAVEN observes energy-time dispersed electron signatures near Martian crustal magnetic fields
- Electrons injected into closed field lines are subsequently dispersed by magnetic drift
- Bursty, sometimes periodic, dispersion signatures suggest dynamic injection processes

Correspondence to:
Y. Harada,
haraday@ssl.berkeley.edu

MAVEN observations of energy-time dispersed electron signatures in Martian crustal magnetic fields

Y. Harada[1], D. L. Mitchell[1], J. S. Halekas[2], J. P. McFadden[1], C. Mazelle[3,4], J. E. P. Connerney[5], J. Espley[5], D. A. Brain[6], D. E. Larson[1], R. J. Lillis[1], T. Hara[1], R. Livi[1], G. A. DiBraccio[5], S. Ruhunusiri[2], and B. M. Jakosky[6]

[1]Space Sciences Laboratory, University of California, Berkeley, California, USA, [2]Department of Physics and Astronomy, University of Iowa, Iowa City, Iowa, USA, [3]CNRS, IRAP, Toulouse, France, [4]Paul Sabatier University, Toulouse, France, [5]NASA Goddard Space Flight Center, Greenbelt, Maryland, USA, [6]Laboratory for Atmospheric and Space Physics, University of Colorado Boulder, Boulder, Colorado, USA

Abstract Energy-time dispersed electron signatures are observed by the Mars Atmosphere and Volatile EvolutioN (MAVEN) mission in the vicinity of strong Martian crustal magnetic fields. Analysis of pitch angle distributions indicates that these dispersed electrons are typically trapped on closed field lines formed above strong crustal magnetic sources. Most of the dispersed electron signatures are characterized by peak energies decreasing with time rather than increasing peak energies. These properties can be explained by impulsive and local injection of hot electrons into closed field lines and subsequent dispersion by magnetic drift of the trapped electrons. In addition, the dispersed flux enhancements are often bursty and sometimes exhibit clear periodicity, suggesting that the injection and trapping processes are intrinsically time dependent and dynamic. These MAVEN observations demonstrate that common physical processes can operate in both global intrinsic magnetospheres and local crustal magnetic fields.

1. Introduction

Mars lacks a global dynamo magnetic field, but it possesses a significant atmosphere and inhomogeneous and locally strong crustal magnetic fields [*Acuña et al.*, 1999; *Connerney et al.*, 2005]. As a result, an induced magnetosphere is formed by the mass-loaded solar wind and the pileup of the interplanetary magnetic field over the conductive ionosphere [e.g., *Nagy and et al.*, 2004]. Globally, the Martian induced magnetosphere is categorized into a different class of solar wind obstacles from intrinsic magnetospheres such as that of the Earth [*Barabash*, 2012]; locally, however, Martian crustal magnetic fields exhibit remarkably similar features to those seen in intrinsic magnetospheres, including auroral processes [*Lundin et al.*, 2006; *Brain and Halekas*, 2012].

The presence of locally strong crustal magnetic fields in the absence of a global dynamo magnetic field gives rise to complex magnetic field topology in the vicinity of Mars. Field lines around Mars can be categorized into three types: closed field lines with both ends rooted in Mars' atmosphere; open field lines connected to the atmosphere at one end and to interplanetary space at the other end; and detached field lines with both ends extended to interplanetary space. Each type of field line topology displays distinct classes of pitch angle distributions of ~100 eV electrons because these electrons are typically magnetized in the Martian environment (i.e., their gyroradii are small compared with local magnetic field curvature radii) [*Lillis et al.*, 2008]. In the nightside magnetosphere, closed field lines contain trapped electrons with two-sided loss cones or no detectable suprathermal electrons (so-called plasma voids), while open field lines are associated with one-sided loss cones consisting of incident and adiabatically reflected and backscattered electrons [*Brain et al.*, 2007; *Lillis et al.*, 2008]. Auroral electrons with peaked energy spectra are produced by electron injection along open field lines [*Brain et al.*, 2006]. The magnetic field topology at certain places above Mars may not be constant over time but can be changed by magnetic reconnection as suggested by in situ measurements of reconnection signatures [*Eastwood et al.*, 2008; *Harada et al.*, 2015].

A wealth of previous observations demonstrate that the Mars-solar wind system is dynamic in response to variations in the upstream solar wind, interplanetary magnetic field, crustal field locations with respect to the solar wind flow, and other properties [e.g., *Brain*, 2006; *Futaana et al.*, 2006; *Dubinin et al.*, 2009, 2012;
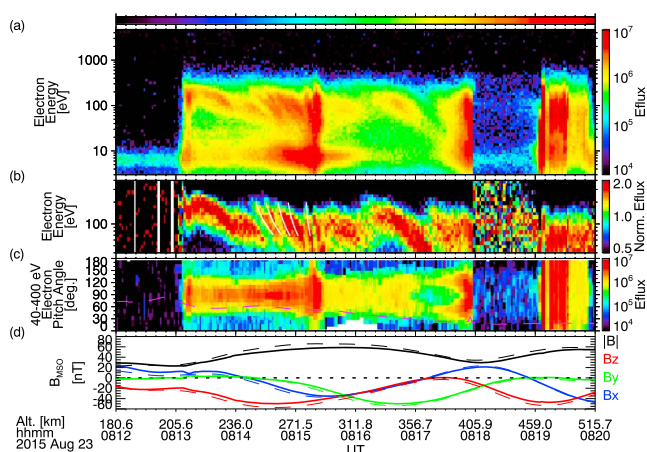
Figure 1. Time series data from MAVEN on 23 August 2015. Electron energy spectra from SWEA in units of (a) differential energy flux (eV/cm^2/s/str/eV) and (b) normalized for each time step by the average differential energy flux between 40 and 400 eV; (c) pitch angle distributions (PADs) of 40–400 eV electrons in units of differential energy flux; and (d) magnetic field measured by MAG (solid) and predicted from a crustal field model (dashed) [*Morschhauser et al.*, 2014]. The energy spectra are obtained by taking a weighted average of all azimuth-elevation bins [*Mitchell et al.*, 2016]. The MAVEN altitude, based on a uniform Mars radius (R_M = 3389.9 km), is denoted in the time label. The white curves in Figure 1b shows the expected $1/E$ dependence of the drift dispersion. The magenta dashed line in Figure 1c shows the loss cone angle predicted from the crustal field model assuming an electron absorbing altitude of 170 km. The horizontal color bar on the top corresponds to the colors of the MAVEN orbit in Figures 2 and 4. The white areas in Figure 1c correspond to pitch angles out of the SWEA field of view or blocked by the spacecraft.

Hara et al., 2011; *Diéval et al.*, 2013]. Recently, initial results from the Mars Atmosphere and Volatile EvolutioN (MAVEN) mission [*Jakosky et al.*, 2015] have revealed and characterized a number of time-dependent phenomena in the Martian magnetosphere, including time-dispersed ion signatures [*Halekas et al.*, 2015], low-frequency waves [*Ruhunusiri et al.*, 2015], and magnetotail dynamics [*DiBraccio et al.*, 2015]. This paper presents MAVEN observations of a new class of dynamic phenomena in the Martian magnetosphere: energy-time dispersed electron signatures in the vicinity of Martian crustal magnetization.

2. Observations

We present both case and statistical studies based on the electron and magnetic field data obtained by the Solar Wind Electron Analyzer (SWEA) [*Mitchell et al.*, 2016] and magnetometer (MAG) [*Connerney et al.*, 2015] instruments on board MAVEN. Figure 1 depicts a series of energy-time dispersed electron signatures observed in the nightside Martian magnetosphere. As seen in the electron energy-time spectrograms in units of non-normalized and normalized differential energy flux (Figures 1a and 1b), the peaks in the energy spectra move toward lower energies from ∼200 eV down to ∼50 eV. These "falling tones" are observed recurrently during this time interval; for example, we observe five quasi-periodic consecutive dispersion signatures starting at 08:14:20, 08:14:30, 08:14:42, 08:14:52, and 08:15:10 UT as indicated by the white curves in Figure 1b. It is worth noting that we observe short bursts of "vertical" peaked spectra at 08:15:22 and 08:17:54 following the falling tone dispersions.
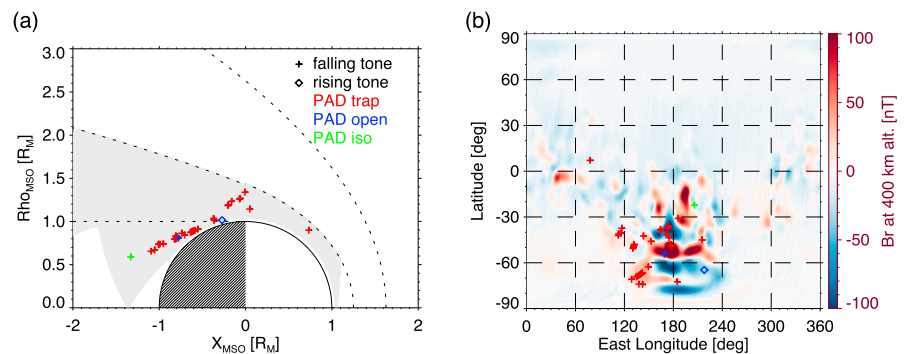
These energy-time dispersed electron signatures exhibit characteristic pitch angle distributions (PADs) for trapped electrons. Figure 1c shows PADs of 40–400 eV electrons. When the dispersion signatures are observed at 08:13:26–08:17:00 UT, we observe two-sided loss cones (i.e., flux depletion at both parallel and antiparallel directions). This type of electron PADs implies that electrons are trapped on closed field lines, which are connected to the collisional atmosphere at both ends [*Brain et al.*, 2007]. Besides, the observed loss cone angles are in good agreement with the theoretical cutoff angles (the magenta dashed line in Figure 1c) predicted from the ratios of magnetic field magnitude at the MAVEN location and at an electron absorbing altitude of 170 km [*Lillis et al.*, 2008] in a crustal field model [*Morschhauser et al.*, 2014]. This indicates that the observed PADs are produced by the adiabatic reflection and absorption of electrons instead of the effects of perpendicular heating. We also note that the presence of narrow one-sided loss cones at 08:19:24 indicates open field lines, on which part of the incident electrons are mirrored back by converging field lines, and the others are absorbed/backscattered by the atmosphere.
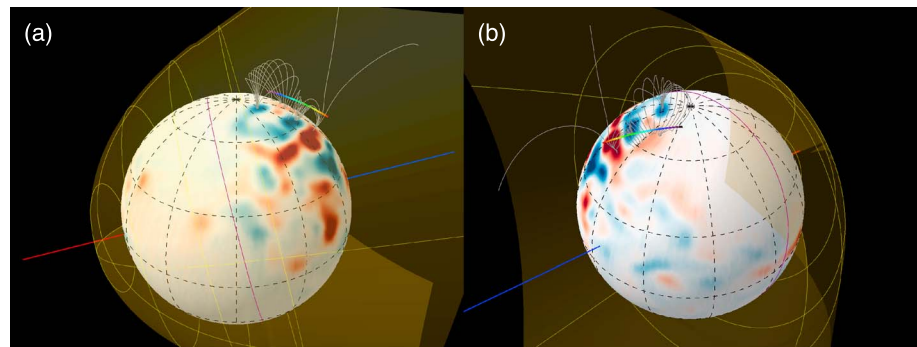
Figure 2. Three-dimensional (3-D) views of the field line topology (gray lines) [*Morschhauser et al.*, 2014], nominal magnetic pileup boundary (yellow surface) [*Trotignon et al.*, 2006], and MAVEN orbit (rainbow line) during the time interval shown in Figure 1. The radial component of the crustal magnetic field at ~400 km altitude [*Connerney et al.*, 2001] is projected on the Mars surface (R_M = 3389.9 km) with the linear color scale from −100 nT to +100 nT (the same color scale as Figure 3b). The red and blue bars indicate the Sun and anti-Sun directions, and the purple line on the surface denotes the day-night terminator. Note that these figures are viewed from the Southern Hemisphere and the South Pole is located on the upper side.

Figure 1d shows magnetic fields observed by MAG (solid lines) and those predicted by the crustal field model (dashed lines) [*Morschhauser et al.*, 2014]. The observed and predicted fields are consistent, indicating that the crustal fields dominate over the external fields at the MAVEN position. Figure 2 shows the observation geometry, including the magnetic field line tracing based on the crustal field model (gray lines) from the MAVEN orbit (rainbow line with colors corresponding to the time scale shown on the top of Figure 1), and the nominal magnetic pileup boundary (yellow surface) [*Trotignon et al.*, 2006]. The crustal field model predicts that MAVEN first crosses the closed field lines near the geographic South Pole deep within the Martian induced magnetosphere and then moves to the open field lines near the end of this time interval. This prediction is basically consistent with the electron PAD observations, suggesting that the magnetic field topology at this time and location is mostly determined by crustal fields. The field line topology inferred from the electron PADs and crustal field model indicates that the dispersed electrons are trapped on closed field lines above Martian crustal magnetization.

We conduct a statistical survey of dispersed electron events. Here we focus on dispersion signatures observed within the Martian magnetosphere and do not discuss upstream and sheath phenomena. We visually scanned electron energy-time spectrograms obtained by SWEA from November 2014 to August 2015 and identified

Figure 3. Spatial distributions of energy-time dispersed electron events in (a) cylindrical MSO and (b) geographic coordinates. The plus signs denote "falling tone" events, in which the peak energy decreases with time, while the diamonds represent "rising tone" events with increasing peak energies. Types of electron PADs are shown in symbol colors: trapped (red), open (blue), and isotropic (green) PADs. The gray area in Figure 3a indicates the searched area covered by the MAVEN orbits below the nominal magnetic pileup boundary [*Trotignon et al.*, 2006]. The background color contour in Figure 3b shows the radial component of the crustal magnetic field at ~400 km altitude [*Connerney et al.*, 2001].

37 discrete dispersion signatures (i.e., rising/falling tones) in the 50–1000 eV range. The event list is provided in the supporting information (Table S1). Some of the electron dispersion signatures are observed as isolated events, while others are grouped together and sometimes exhibit clear periodicity. Figure 3 shows the spatial distributions of the identified dispersion events in cylindrical Mars Solar Orbital (MSO) and geographic coordinates. The dispersion events are found at relatively low altitudes $< \sim 1500$ km mainly on, but not limited to, the nightside of Mars (Figure 3a). All but one are characterized by falling tones (crosses) instead of rising tones (diamonds). The majority of the events are associated with "trapped" PADs (two-sided loss cones/conics, indicated by red), and we find only two events with "open" PADs (one-sided loss cones, indicated by blue) and one "isotropic" event (green). Figure 3b shows that the events are clustered near strong crustal fields in the Southern Hemisphere. In summary, most of the energy-time dispersed electron signatures identified so far are characterized by falling tones with trapped PADs and are distributed near strong crustal magnetization.

3. Interpretation

The predominance of falling tones (the peak energy decreases with time) suggests that the majority of the observed dispersion events are more consistent with intrinsically time-dependent phenomena rather than spatial structures encountered by moving spacecraft, which would result in roughly equal numbers of rising and falling tones. Also, the association of the dispersion events with trapped PADs and strong crustal fields suggests that the closed field line topology is an important factor for the dispersion mechanisms. Based on these observations, we interpret the energy-time dispersed electron signatures by considering the drift dispersion of hot electrons that are injected impulsively and locally on closed field lines with broad energies. Such injection and dispersion of charged particles have been observed in the terrestrial inner magnetosphere for decades [e.g., *Konradi*, 1967; *DeForest and McIlwain*, 1971; *Greenspan et al.*, 1985; *Birn et al.*, 1997; *Angelopoulos et al.*, 2008]. As the magnetic drift velocity depends on the particle energy (the ∇B drift velocity is proportional to the perpendicular energy and the curvature drift velocity is proportional to the parallel energy), higher-energy electrons drift faster than lower energy electrons. If broad-energy particles are injected with limited spatial and temporal scales, a spacecraft at a distant place on the particles' drift paths will observe a discrete dispersion signature in which higher-energy particles arrive first, followed by lower energy particles. The expected $t \propto 1/E$ dependence by the magnetic drift dispersion is shown by the white lines for the five quasi-periodic dispersion signatures in Figure 1b, which roughly match the arrival of dispersed electrons.

Here we investigate the electron motion on closed field lines above Martian crustal magnetic sources by conducting test particle tracing in the *Morschhauser et al.* [2014]'s crustal magnetic field model with zero electric fields. We note that the $\mathbf{E} \times \mathbf{B}$ drift is independent of energy and perpendicular electric fields cannot account for the energy dispersion. Parallel electric fields are also unlikely to be responsible for the energy dispersion given the trapped nature of the dispersed electrons. We backtrace 200 eV and 70 eV electrons of the dispersion signatures shown in Figure 1 from the observed time and location by numerically solving the full equation of motion. Assuming that these electrons are injected in the same flux tube at the same time, we can estimate the injection time and location by identifying the time when the backtraced 200 eV and 70 eV electrons are bouncing on the same field line. In practice, the two field lines may not exactly match because the 200 eV and 70 eV electrons observed at different times and locations by a moving spacecraft may not drift on the same shell and not originate from exactly the same place. Also, the actual magnetic field may be deviated from the crustal field model by plasma currents. Nevertheless, the crustal field model should provide with first-order characteristics of the magnetic field topology as demonstrated by its consistency with the observed electron PADs.

Figure 4a shows the estimated injection field lines (yellow lines) for the first of the five quasi-periodic dispersion signatures (the first white curve in Figure 1b) as well as the trajectories of 200 eV (red) and 70 eV (blue) electrons at the injection time. The 200 eV and 70 eV electrons that are injected on nearly the same field lines travel back and forth between the mirror points, dispersed by different magnetic drift velocities at later times as shown in Figures 4b and 4c. The 200 eV electrons drift faster in the azimuthal direction of the closed loops and arrive at MAVEN earlier (just after the time of Figure 4c) compared to the arrival of the more slowly drifting 70 eV electrons (just after the time of Figure 4d). Similar results are obtained for the other four dispersion signatures, and a full movie showing the 200 eV and 70 eV electron motion of the five quasi-periodic dispersion signatures is provided in the supporting information (Movie S1).
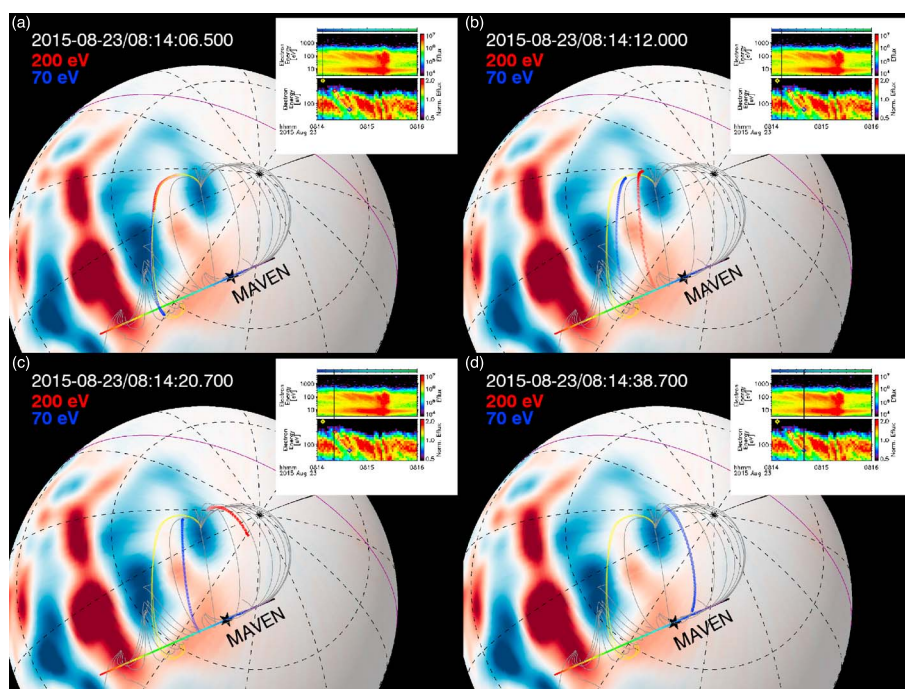
Figure 4. Snapshots of 200 eV (red) and 70 eV (blue) electron trajectories based on backtracing of the dispersed electrons with an initial pitch angle of 80° in the *Morschhauser et al.*'s [2014] crustal field model. The vertical black bar in the spectrograms indicate the time of each snapshot. The yellow diamonds in the spectrograms denote the estimated injection time, and the yellow traces in the 3-D plot show the estimated injection field lines. The red and blue diamonds in the spectrograms show the arrival times of the 200 eV and 70 eV electrons. Figures 4c and 4d show the times just before the 200 eV and 70 eV electron arrival at MAVEN, respectively.

4. Implications

As we have presented, the properties of typical energy-time dispersed electron events observed by MAVEN can be explained by the injection of broad-energy electrons and the subsequent magnetic drift dispersion of trapped electrons on closed field lines. This drift dispersion is essentially the same physical process for the well-known energy-time dispersion signatures of charged particles produced by substorm-associated injections of hot plasma into the Earth's inner magnetosphere [e.g., *Konradi*, 1967; *DeForest and McIlwain*, 1971; *Greenspan et al.*, 1985; *Birn et al.*, 1997; *Angelopoulos et al.*, 2008]. One remarkable difference of Mars from Earth is that the closed field line topology is provided by crustal fields, not by intrinsic dynamo fields. The MAVEN observations of the drift dispersed electrons provide another demonstration that common physical processes can operate in either a global dynamo field or local crustal fields.

Assuming that the majority of the energy-dispersed electrons are caused by temporal phenomena based on the predominance of falling tones, the discrete, bursty nature of the dispersion signatures suggests that the electron injection must be relatively impulsive and local (i.e., electrons must be injected over a short time period within a small spatial extent in the azimuthal direction of closed loops); otherwise, injected electrons at a certain energy will be observed over a long time period. For example, the widths of the individual dispersion signatures at a certain energy in Figure 1 are on the order of ~10 s, implying injection durations shorter than ~10 s. The bursty injection of hot electrons into closed field lines is most likely due to intrinsically time-dependent and dynamic processes such as transient reconnection. In this sense, the bursts of vertical flux enhancement at 08:15:22 and 08:17:54 in Figure 1a may represent freshly injected and trapped hot electrons. Also, some of the observed dispersion signatures exhibit clear periodicity with typical recurrence periods of 10–100 s (cf. Figure 1 and Table S1), suggesting that ion-scale/MHD waves may be implicated in the injection processes in some cases. The injection and dispersion of hot electrons observed by MAVEN represent one of the dynamic processes operating in Martian crustal magnetic fields and in the Martian-induced magnetosphere.

References

Acuña, M. H., et al. (1999), Global distribution of crustal magnetization discovered by the Mars global surveyor mag/er experiment, *Science*, *284*(5415), 790–793, doi:10.1126/science.284.5415.790.

Angelopoulos, V., et al. (2008), Tail reconnection triggering substorm onset, *Science*, *321*(5891), 931–935, doi:10.1126/science.1160495.

Barabash, S. (2012), Classes of the solar wind interactions in the solar system, *Earth Planets Space*, *64*, 57–59.

Birn, J., M. F. Thomsen, J. E. Borovsky, G. D. Reeves, D. J. McComas, R. D. Belian, and M. Hesse (1997), Substorm ion injections: Geosynchronous observations and test particle orbits in three-dimensional dynamic MHD fields, *J. Geophys. Res.*, *102*(A2), 2325–2341, doi:10.1029/96JA03032.

Brain, D. (2006), Mars global surveyor measurements of the Martian solar wind interaction, *Space Sci. Rev.*, *126*(1–4), 77–112, doi:10.1007/s11214-006-9122-x.

Brain, D., and J. S. Halekas (2012), Aurora in martian mini magnetospheres, in *Auroral Phenomenology and Magnetospheric Processes: Earth And Other Planets*, edited by A. Keiling et al., AGU, Washington, D. C., doi:10.1029/2011GM001201.

Brain, D., et al. (2006), On the origin of aurorae on Mars, *Geophys. Res. Lett.*, *33*(1), L01201, doi:10.1029/2005GL024782.

Brain, D. A., R. J. Lillis, D. L. Mitchell, J. S. Halekas, and R. P. Lin (2007), Electron pitch angle distributions as indicators of magnetic field topology near Mars, *J. Geophys. Res.*, *112*(A9), A09201, doi:10.1029/2007JA012435.

Connerney, J., J. Espley, P. Lawton, S. Murphy, J. Odom, R. Oliversen, and D. Sheppard (2015), The MAVEN magnetic field investigation, *Space Sci. Rev.*, 1–35, doi:10.1007/s11214-015-0169-4.

Connerney, J. E. P., M. H. Acuña, P. J. Wasilewski, G. Kletetschka, N. F. Ness, H. Rème, R. P. Lin, and D. L. Mitchell (2001), The global magnetic field of Mars and implications for crustal evolution, *Geophys. Res. Lett.*, *28*(21), 4015–4018, doi:10.1029/2001GL013619.

Connerney, J. E. P., M. H. Acuña, N. F. Ness, G. Kletetschka, D. L. Mitchell, R. P. Lin, and H. Reme (2005), Tectonic implications of Mars crustal magnetism, *Proc. Natl. Acad. Sci.*, *102*(42), 14,970–14,975, doi:10.1073/pnas.0507469102.

DeForest, S. E., and C. E. McIlwain (1971), Plasma clouds in the magnetosphere, *J. Geophys. Res.*, *76*(16), 3587–3611, doi:10.1029/JA076i016p03587.

DiBraccio, G. A., et al. (2015), Magnetotail dynamics at Mars: Initial MAVEN observations, *Geophys. Res. Lett.*, *42*, 8828–8837, doi:10.1002/2015GL065248.

Diéval, C., G. Stenberg, H. Nilsson, N. J. T. Edberg, and S. Barabash (2013), Reduced proton and alpha particle precipitations at Mars during solar wind pressure pulses: Mars express results, *J. Geophys. Res.*, *118*(6), 3421–3429, doi:10.1002/jgra.50375.

Dubinin, E., M. Fraenz, J. Woch, T. L. Zhang, J. Wei, A. Fedorov, S. Barabash, and R. Lundin (2012), *Geophys. Res. Lett.*, *39*(1), L01104, doi:10.1029/2011GL049883.

Dubinin, E., M. Fraenz, J. Woch, F. Duru, D. Gurnett, R. Modolo, S. Barabash, and R. Lundin (2009), Ionospheric storms on Mars: Impact of the corotating interaction region, *Geophys. Res. Lett.*, *36*, L01105, doi:10.1029/2008GL036559.

Eastwood, J. P., D. A. Brain, J. S. Halekas, J. F. Drake, T. D. Phan, M. Oieroset, D. L. Mitchell, R. P. Lin, and M. Acuña (2008), Evidence for collisionless magnetic reconnection at Mars, *Geophys. Res. Lett.*, *35*(2), L02106, doi:10.1029/2007GL032289.

Futaana, Y., S. Barabash, A. Grigoriev, D. Winningham, R. Frahm, M. Yamauchi, and R. Lundin (2006), Global response of Martian plasma environment to an interplanetary structure: From ENA and plasma observations at Mars, *Space Sci. Rev.*, *126*(1–4), 315–332, doi:10.1007/s11214-006-9026-9.

Greenspan, M. E., D. J. Williams, B. H. Mauk, and C.-I. Meng (1985), Ion and electron energy dispersion features detected by ISEE 1, *J. Geophys. Res.*, *90*(A5), 4079–4089, doi:10.1029/JA090iA05p04079.

Halekas, J. S., et al. (2015), Time-dispersed ion signatures observed in the Martian magnetosphere by MAVEN, *Geophys. Res. Lett.*, *42*, 8910–8916, doi:10.1002/2015GL064781.

Hara, T., K. Seki, Y. Futaana, M. Yamauchi, M. Yagi, Y. Matsumoto, M. Tokumaru, A. Fedorov, and S. Barabash (2011), Heavy-ion flux enhancement in the vicinity of the Martian ionosphere during CIR passage: Mars express ASPERA-3 observations, *J. Geophys. Res.*, *116*, A02309, doi:10.1029/2010JA015778.

Harada, Y., et al. (2015), Magnetic reconnection in the near-Mars magnetotail: MAVEN observations, *Geophys. Res. Lett.*, *42*, 8838–8845, doi:10.1002/2015GL065004.

Jakosky, B. M., J. M. Grebowsky, J. G. Luhmann, and D. A. Brain (2015), Initial results from the MAVEN mission to Mars, *Geophys. Res. Lett.*, *42*, 8791–8802, doi:10.1002/2015GL065271.

Konradi, A. (1967), Proton events in the magnetosphere associated with magnetic bays, *J. Geophys. Res.*, *72*(15), 3829–3841, doi:10.1029/JZ072i015p03829.

Lillis, R. J., D. L. Mitchell, R. P. Lin, and M. H. Acuña (2008), Electron reflectometry in the Martian atmosphere, *Icarus*, *194*(2), 544–561, doi:10.1016/j.icarus.2007.09.030.

Lundin, R., et al. (2006), Plasma acceleration above Martian magnetic anomalies, *Science*, *311*(5763), 980–983, doi:10.1126/science.1122071.

Mitchell, D. L., et al. (2016), The MAVEN solar wind electron analyzer, *Space Sci. Rev.*, doi:10.1007/s11214-015-0232-1.

Morschhauser, A., V. Lesur, and M. Grott (2014), A spherical harmonic model of the lithospheric magnetic field of Mars, *J. Geophys. Res.*, *119*(6), 1162–1188, doi:10.1002/2013JE004555.

Nagy, A., et al. (2004), The plasma environment of Mars, *Space Sci. Rev.*, *111*(1–2), 33–114, doi:10.1023/B:SPAC.0000032718.47512.92.

Ruhunusiri, S., J. S. Halekas, J. E. P. Connerney, J. R. Espley, J. P. McFadden, D. E. Larson, D. L. Mitchell, C. Mazelle, and B. M. Jakosky (2015), Low frequency waves in the Martian magnetosphere and their response to upstream solar wind driving conditions, *Geophys. Res. Lett.*, *42*, 8917–8924, doi:10.1002/2015GL064968.

Trotignon, J., C. Mazelle, C. Bertucci, and M. Acuña (2006), Martian shock and magnetic pile-up boundary positions and shapes determined from the hobos 2 and Mars global surveyor data sets, *Planet. Space Sci.*, *54*(4), 357–369, doi:10.1016/j.pss.2006.01.003.